International Journal of Engineering Trends and Technology
ISSN: 2231 – 5381 / https://doi.org/10.14445/22315381/IJETT-V71I2P214

Volume 71 Issue 2, 111-120, February 2023

Original Article

Detection and Removal of Climatic Noise from Remotely Sensed Images through LANDSAT8/OLI/TIRS with Ground Truth Validation using MLC, MDC, and RF

Renuka Sandeep Gound[1], Sudeep D. Thepade[2]

[1]*Computer Science and Engineering, New Horizon College of Engineering, Bangalore, Karnataka.*
[1]*Research Scholar in Computer Engineering, Pimpri Chinchwad College of Engineering, Maharashtra, India.*
[2]*Computer Engineering, Pimpri Chinchwad College of Engineering, Maharashtra, India.*

[1]*Corresponding Author : renuka060182@gmail.com*

Received: 12 September 2022 Revised: 09 February 2023 Accepted: 14 February 2023 Published: 25 February 2023

Abstract *- The remotely sensed images acquired through the satellites play a significant role in various crop management applications in agriculture, security and defense activities, monitoring disasters, and change detection on Land with LULC. Sometimes these images carry the climatic noise occurrences over the ground surface, which may occlude the regions. This article presents a novel method for detecting and removing climatic noise from remotely sensed images acquired from LANDSAT8/OLI/TIRS with accurate Ground Truth Validation. The proposed system identifies the climatic noise by using the combination of empirical pixel values of the Quality Assessment Band and Band-9 of LANSAT8/OLI/TIRS. Land cover obtained is classified using Maximum Likelihood Classifier (MLC), Random Forest Classifier (RF) and Minimum Distance Classification (MDC), with NDVI and NDWI thresholds. The image is reconstructed after collecting and replacing the pixel values, with the influence of Climatic Noise using the reference image. The performance measurements used for the proposed system depict the desired results. The Standard Error (SE) is almost close to zero for all the scenes. User Accuracies and Producer Accuracies are also more than 90 %. The K-hat statistics are also closer to one for all scenes, and the overall accuracy achieved is also more than 90% for most of the scenes. It is seen from the statistics and findings achieved with the proposed system; the ground cover obtained with the proposed system can be further utilised in the applications of the remote sensing field.*

Keywords *- Climatic Noise, Maximum Likelihood Classifier (MLC), Minimum Distance Classification (MDC), Normalised Difference Vegetation Index (NDVI), Normalised Difference Water Index (NDWI), Random Forest Classifier (RF).*

1. Introduction

The proposed system acquires the scene from the satellite LANDSAT8/OLI/TIRS, having an occurrence of climatic noises. The proposed system aims to identify these noisy pixels by using their spectral differences from the material available on the scene. After the reduction in climatic noise, ground data is validated using the error matrix obtained. The proposed system uses the Maximum Likelihood Classification, Minimum Distance Classification and Random Forest Classification to classify the land cover with Water, Vegetation, Built-up, and Soil classes. The classification is enhanced by applying NDVI and NDWI indexes to segment the classes more accurately. The boundaries or edges of the elements present on land cover, made with this admixing, may help the better presentation of ground truth with proper segmentation. The proposed system is developed considering the climatic noise of Cirrus, Cloud and Shadows, which may hide ground truth regions. It has been observed that many pixels are not recognised during classification using the only "Quality analysis band". So, to identify the cirrus pixels more precisely and to avoid the burring of edges of cloud area boundaries proposed system of cirrus detection and removal used the combination of band-9 and quality analysis band, which makes the effective detection of cirrus pixels and avoids the misclassification of cirrus, cloud, and shadow pixel. Following is the block schematic (fig.1) of the proposed system to identify and reduce the climatic noise from scenes captured with LANDSAT satellite by Detection and Removal of Climatic Noise with Ground Truth Validation using MLC, MDC, and RF.

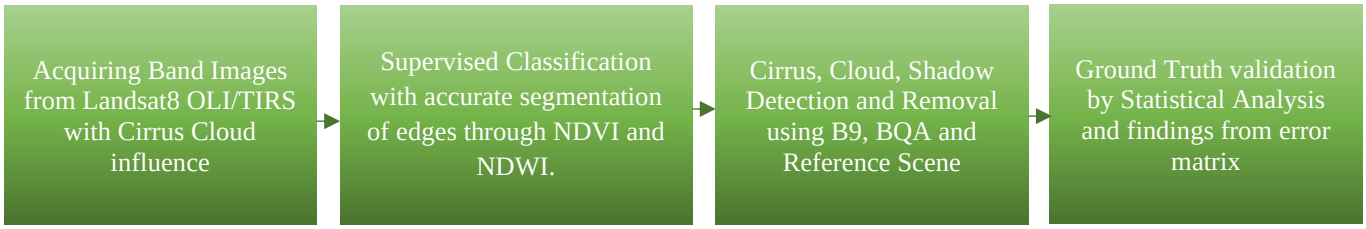

Fig. 1 Block Schematic of Cirrus Detection and Removal

The proposed system is motivated by the image processing applications [27] to [31] presented in various fields. Remote sensing applications aim to take images obtained through satellites and aerial photography. The existing work conducted by the researchers has also stated the significance of the detection and removal of climatic noise in the field of remote sensing. Daniel Schlapfer et al. [1] have developed the elevation-based cirrus removal technique, which is mainly observed over midlatitudes and tropical regions. As a result, many of the images were produced.

Bo-Cai Gao et al. [2] utilized the band-9 (1.375 m) of Landsat8/OLI/TIRS for the detection of cirrus pixels and masked the thin cirrus-influenced area. This paper presented the technique on three datasets Landsat8/OLI, with the combined NIR and SWIR data. Suggested to use the empirical data for more effective results. Binxing Zhou et al. [3] implemented the RTM algorithm with b-9 to reduce the cirrus with Landsat8/OLI. Yang Shen et al. [4] used ICA with b-9 to remove the influence of cirrus. Ratna Prastyani et al. [5] used image-based techniques to correct the cirrus cloud from Landsat8/OLI. Jing Wei et al. [6] implement an advanced RFmask algorithm by combining the pixels from the Random Forest algorithm and segmentation with the SEEDs method. Nan Ma et al. [7] implemented CNN to detect clouds and correctly classify pixel values. Lam Pham et al. [8] developed a classification-based application to detect the cloud pixels from NWPU-RESISC-45. The cloud regions are improved with GAN based method of MEcGANs proposed by Cengis Hasan et al. [9]. Sergii Skakun et al. [10] Presented CMIX for Landsat-8, Sentinel-2 Z. Li et al. [11] Solution to suppress the problems of omission or commission errors in the removal of cloud.

Chepfer, H et. al. [12] used the Rayleigh method with POLDER-1 to validate the attributes related to the cirrus cloud. Amy Tal Rose et al. [13] presented an ACE and MF to elaborate on replacing the noise pixels with AVIRIS using the reference image. Tran Thi Ngoc Trieu et al. [14] analyzed the importance of cirrus and aerosol with GOSAT. Qiang Li et al. [15] used LIDAR to observe the properties of the Cirrus cloud during the ten years span.

Ali S et al. [16] observed the seasonal change in west Bengal using the LIDAR sensor. Lidar (MPL). Liang, S et. al. [17] corrected the vegetation region with the SAV method from Sentinel by detecting and removing the cirrus effect. Junmei Kang et al. [18] used GEE to label the data to present the clouds and extract the regions of paddy plants with SENTINEL-1 and SENTINEL-2. The cirrus cloud had been detected and removed from the sentinel-2, and ground truth validation performed by supervised classification and diminishing the cirrus, cloud and shadow with MDC is presented by Renuka Gound et al. [19][33]

2. Materials and Methods

LC08_L1TP_144046_20180206_20200902_02_T1 is the product id of the targeted scene. The scene was acquired on 6th February 2018 (Scene-1) [24]. The cloud coverage of the scene is 45.56%. The scene is having influenced by various climatic noises, mainly clouds, cirrus clouds, and shadows. C08_L1TP_144046_20180222_20200902_02_T1 is the second targeted image. This scene was acquired on 22nd February 2018 (Scene-2) [32], which can be utilized as a reference image to remove the climatic noise from the first targeted image. The cloud coverage on the scene is 0.04%.

LC08_L1TP_144046_20180411_20201015_02_T1 is the third targeted image. This scene was acquired on 11th April 2018 (Scene-3) [26], which can be utilized as a reference image to remove the climatic noise from the first as well as the second targeted image. The cloud coverage on the scene is 2.66%. To identify the cirrus pixels more precisely, the combination of band-9 and quality analysis band which makes the effective detection of cirrus pixels, along with the determination of cloud and shadow effect over the scene. As it has been observed while using the only quality analysis band, most of the pixels which carry the information of cirrus, cloud and shadow are left out. The image was acquired on 6th February 2018 with 45.56% cloud cover (Scene-1). The land cover is categorized by using the training input containing 43 ROIs (Region of Interests). The image Acquired on 22nd February 2018 with 0.04% cloud cover (Sccene-2) is classified with training input of 174 ROIs as the cloud coverage is less, leading to better land cover categorization. This classified land cover is significant for removing climatic noise from scene-1. The image acquired on 11th April 2018 with 2.66% cloud cover (Scene-3) is classified by using the training input containing 43 ROIs. With the above-mentioned parameters, the scenes are classified using MLC, MDC, and RF. NDVI (Normalized Difference Vegetation Index) and NDWI (Normalized Difference Water Index) are applied to highlight the boundaries of the Vegetation area and water area.

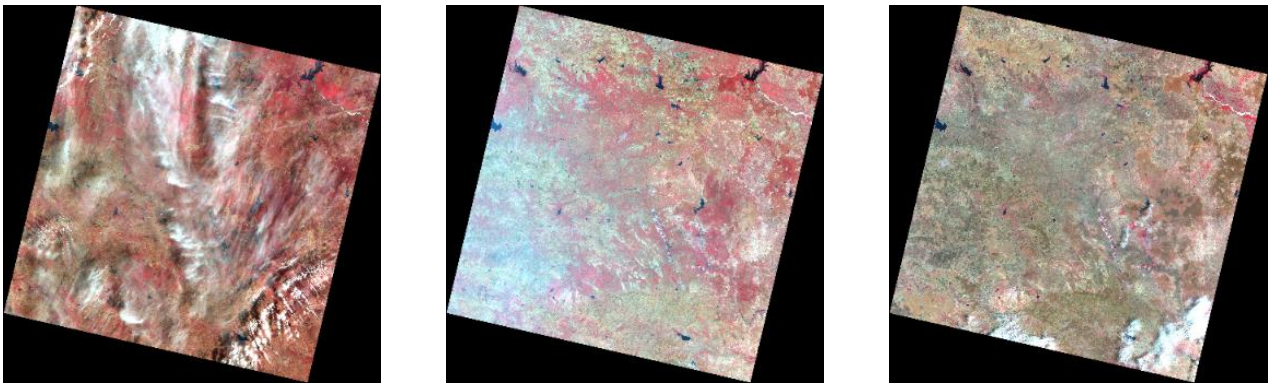

(a) Scene-1 **(b) Scene-2** **(c) Scene-3**

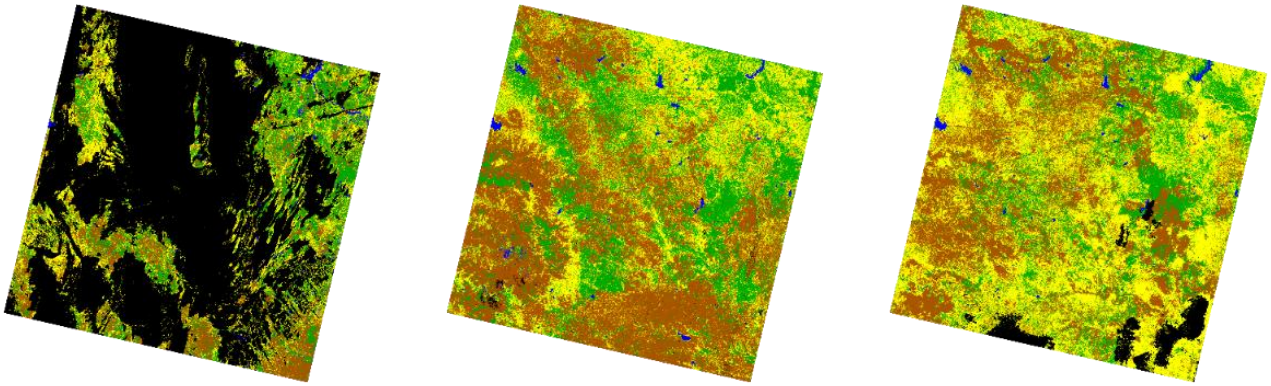

(d) Masking cirrus, cloud and shadow pixels by combining QA and B-9 with MLC

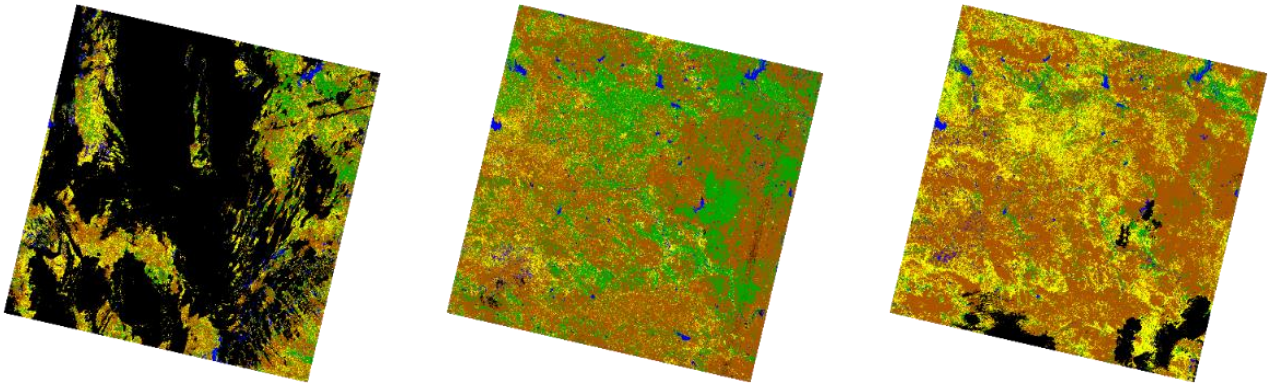

(e) Masking cirrus, cloud and shadow pixels by combining QA and B-9 with MDC

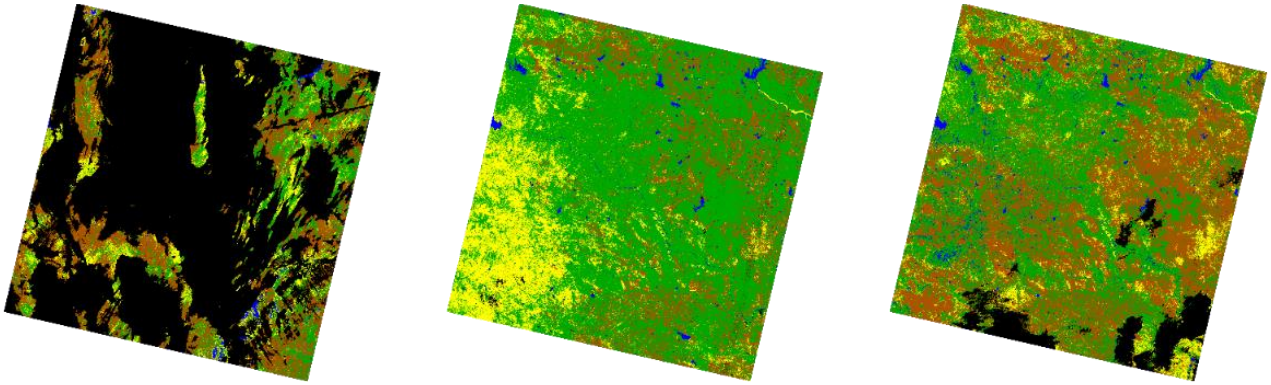

(f) Masking cirrus, cloud and shadow pixels by combining QA and B-9 with RF

Fig. 2 Masking cirrus, cloud and shadow pixels.

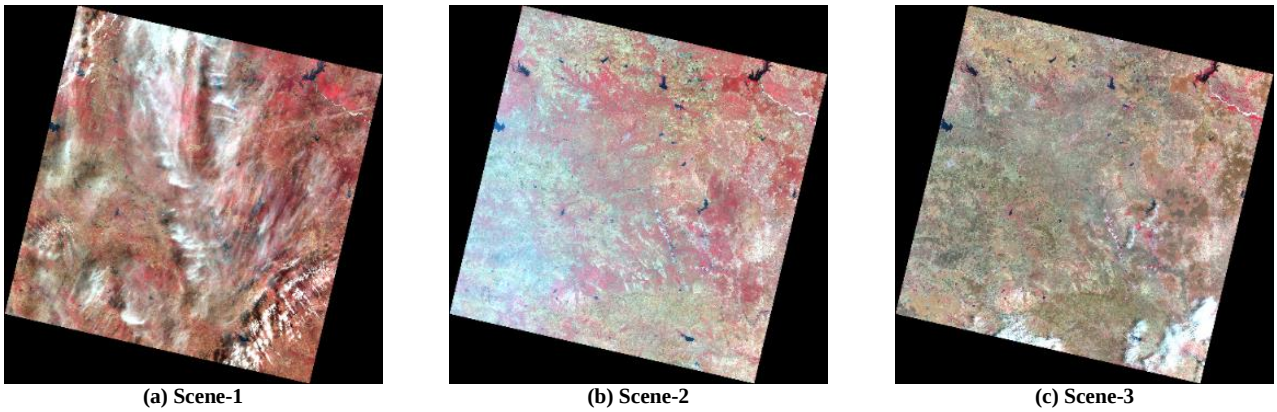

(a) Scene-1 **(b) Scene-2** **(c) Scene-3**

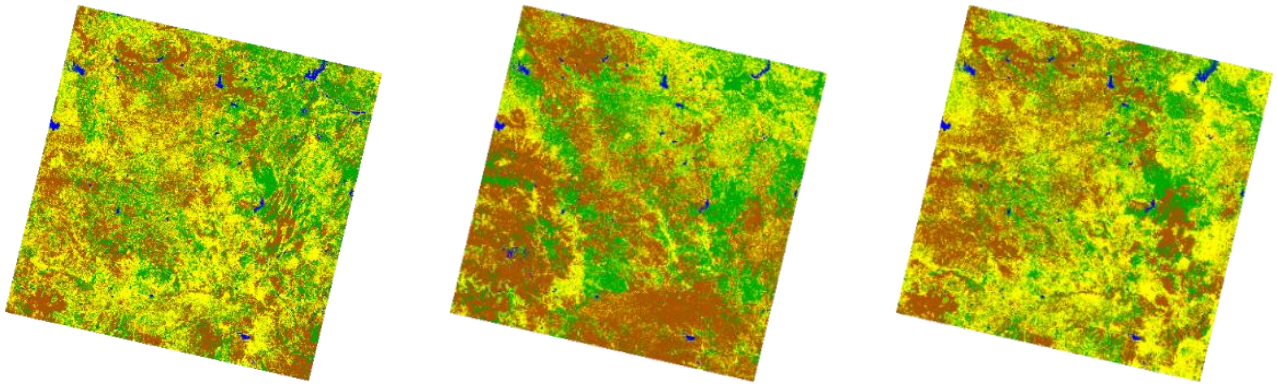

(d) Removal of cirrus, cloud and shadow pixels by combining QA and B-9 with MLC

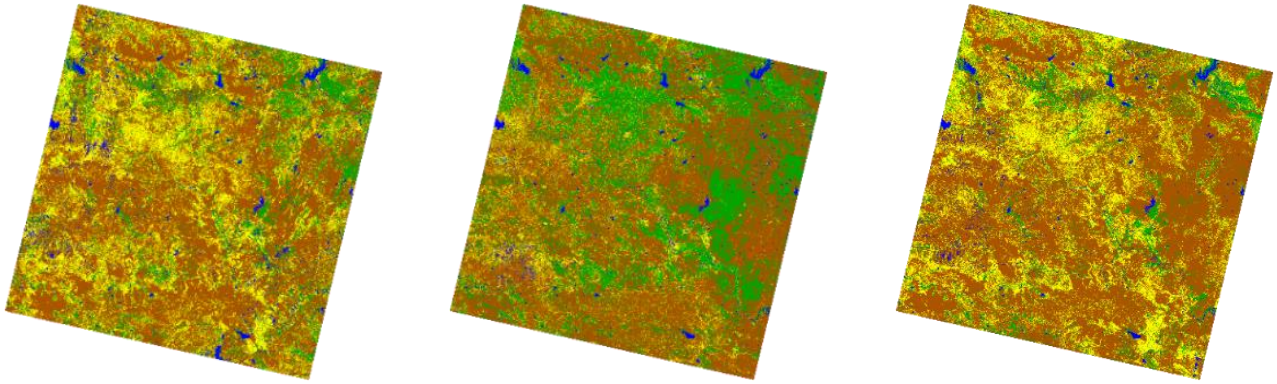

(e) Removal of cirrus, cloud and shadow pixels by combining QA and B-9 with MDC

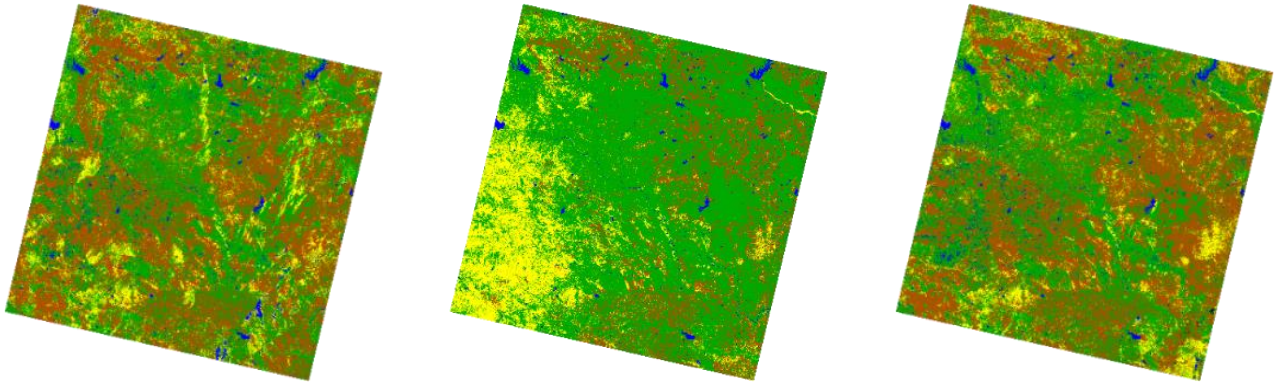

(f) Removal of cirrus, cloud and shadow pixels by combining QA and B-9 with RF

Fig. 3 Removal of cirrus, cloud and shadow pixels

The calculated NDVI threshold selected for vegetation is a value greater than 0.5, and the water index for NDWI is the values greater than zero, i.e., all positive values, to fix the boundaries of these areas. The proposed system combines pixel values of climatic noise associated with QA and Band-9; These pixel values are masked for the left-out pixels from classification. Then with the reference image, all masked pixels are replaced to reconstruct the climatic noise-free image.

Fig. 3 displays the reconstructed classification maps for scene-1, scene-2 and scene-3. After removing climatic noise from classified images, ground truth needs to be checked for further applicability. Therefore, an error matrix is used to evaluate the exactness of ground truth. The following section explains the statistical analysis and findings of the proposed system.

3. Results and Discussion

Table 1. Statistics with QA, B9 and MLC

Class	Water	Vegetation	Built-up	Soil
Scene-1 Statistics				
SE	0.0	0.0	0.0	0.0
PA	67.6	95.9	95.9	93.8
UA	99.9	90.6	93.5	98.7
K-hat	1.0	0.9	0.9	1.0
Scene-2 Statistics				
SE	0.0	0.0	0.0	0.0
PA	82.0	93.3	97.1	100.0
UA	100.0	99.4	99.4	94.1
K-hat	1.0	1.0	1.0	0.9
Scene-3 Statistics				
SE	0	0	0	0
PA	100	86	100	100
UA	100	100	99	91
K-hat	1	1	1	1

Table 2. Statistics with QA, B9 and MDC

Class	Water	Vegetation	Built-up	Soil
Scene-1 Statistics				
SE	0.0	0.0	0.0	0.0
PA	99.3	93.7	97.8	99.9
UA	99.7	99.3	99.9	97.4
K-hat	1.0	1.0	1.0	0.9
Scene-2 Statistics				
SE	0.0	0.0	0.0	0.0
PA	70.4	99.8	100.0	99.9
UA	100.0	96.4	100.0	99.9
K-hat	1.0	1.0	1.0	1.0
Scene-3 Statistics				
SE	0.0	0.0	0.0	0.0
PA	100.0	100.0	100.0	99.5
UA	100.0	99.2	99.1	100.0
K-hat	1.0	1.0	1.0	1.0

Table 3. Statistics with QA, B9 and RF

Class	Water	Vegetation	Built-up	Soil
Scene-1 Statistics				
SE	0.0	0.0	0.0	0.0
PA	74.6	93.3	49.9	94.0
UA	100.0	75.0	91.9	89.4
K-hat	1.0	0.6	0.9	0.8
Scene-2 Statistics				
SE	0.0	0.0	0.0	0.0
PA	26.4	77.1	55.5	29.0
UA	100.0	35.2	20.1	99.9
K-hat	1.0	0.1	0.1	1.0
Scene-3 Statistics				
SE	0.0	0.0	0.0	0.0
PA	100.0	100.0	82.4	55.0
UA	85.1	29.4	42.4	99.3
K-hat	0.8	0.2	0.4	1.0

The ground cover (36927.3 Km^2) obtained after removing cirrus, cloud, and shadows are evaluated with an error matrix.

The summarization of the scenes with different accuracy metrics using MLC is given in table 1.

The summarization of the scenes with different accuracy metrics using MDC is given in table 2.

The summarization of the scenes with different accuracy metrics using MDC is given in table 3.

The results obtained with QA, B-9 and RF are good for scene-1, but for scene-2 and scene-3, OA is not more than 80%, and k-hat is also not much closer to 1. So, it needs to add more samples and trees for accurate classification.

The overall accuracy of the ground truth of Scene-1, Scene-2 and Scene-3 is almost above 90 %, and k-hat is also closer to 1 when the system is implemented with QA, B-9, MLC, and MDC.

Table 4. Ground truth Validation with OA and K-hat

Sr. No.	Algorithm	Landsat8/ OLI/ TIRS scenes	Overall accuracy [%]	K-hat
1	Ground truth validation with MLC	**Scene-1**	94.5	0.9
		Scene-2	97.0	1.0
		Scene-3	96.3	0.9
2	Ground truth validation with MDC.	**Scene-1**	98.4	1.0
		Scene-2	98.9	1.0
		Scene-3	99.7	1.0
3	Ground truth validation with RF	**Scene-1**	83.9	0.8
		Scene-2	44.6	0.2
		Scene-3	62.9	0.4

Standard Error (SE) is almost close to zero for all the scenes. Producer Accuracy of the reference map is above 86% except for the Water class in Scene-1; User Accuracy is almost greater than 90%. The K-hat statistics are also closer to one for all scenes. The overall accuracy and k-hat achieved with the proposed system are displayed in table 4.

With the statistics of the scenes resulting from the proposed QA system, B-9, MLC, and MDC can be further applied in remote sensing. One can observe the OA and K-hat obtained with some of the existing systems of MLR, K-NN, SVM and RF in table 5.

The OA (%) and K-hat, the reliability parameter, shown in table 5 for the specified database, can be interpreted as follows

Nguyen, H.T.T [21] displayed the result of the Dry Season (2017-2018) databse. The OA obtained for the dry season database using MLR, ik-NN, SVM, and RF is 68.3%, 72.1%, 73.2%, and 67.7%. The K-Hat 0.7 is obtained with the algorithms applied.

Y. & Yulianti [22] used SEN2COR object-based segmentation over the South Solok database and achieved 91.3% OA and 0.9 K-Hat. Ju and Zeng [23] used RF (Random Forest) algorithm (integrated multi-decision tree classification method) to validate the data on sentinel scenes, which resulted in 75% OA and 0.7 K-Hat. The proposed system performed the experimentations on the LANDSAT8 scenes.

LC08_L1TP_144046_20180206_20200902_02_T1,
LC08_L1TP_144046_20180222_20200902_02_T1,
LC08_L1TP_144046_20180411_20201015_02_T1,

Table 5. Ground truth Validation with Existing Systems

Sr. No.	Algorithm	Scenes	Overall accuracy [%]	K-hat
1	Multinomial Logistic Regression (MLR)	Dry Season (2017-2018) [21]	68.3	0.7
2	Improved k-Nearest Neighbors (ik-NN)		72.1	0.7
3	Support Vector Machine (SVM)		73.2	0.7
4	Random Forests (RF)		67.7	0.7
5	SEN2COR, Object-based Segmentation and Classification	South Solok [22]	91.3	0.9
6	RF (Random Forest) algorithm (integrated multi-decision tree classification method)	SENTINEL-2A Scenes [23]	75	0.7

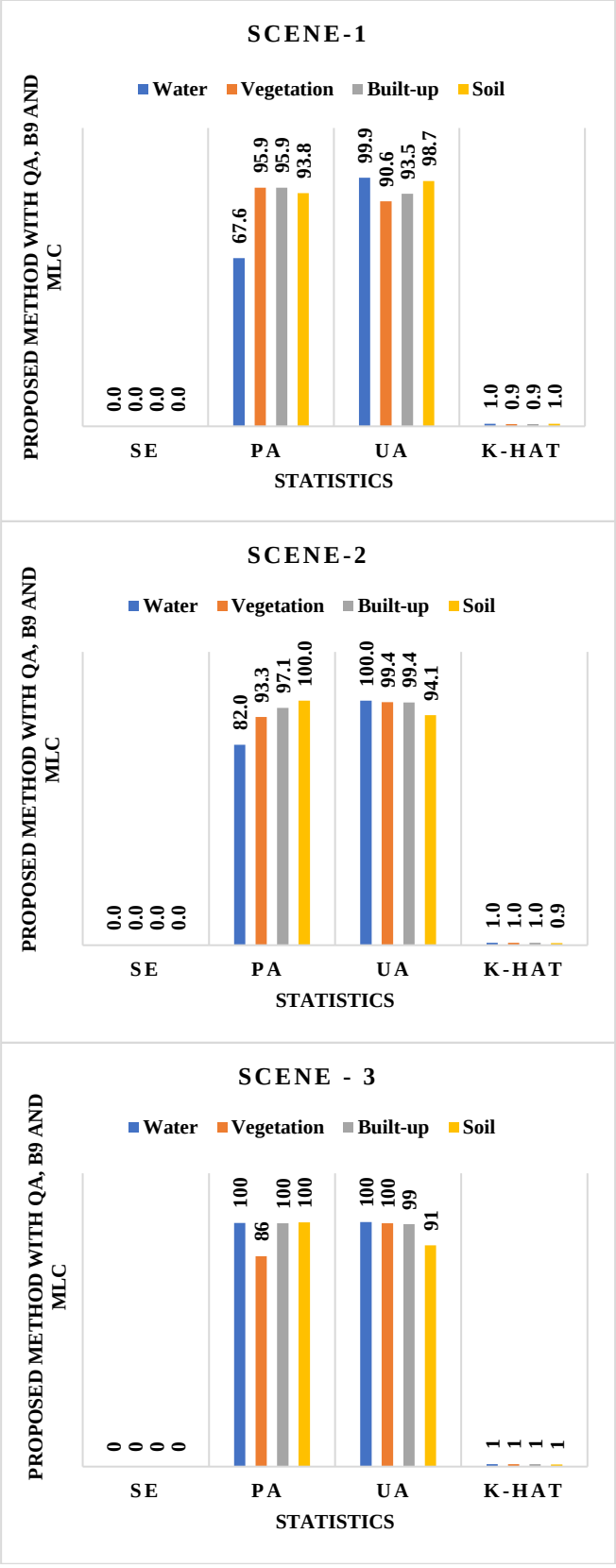

4 (a) Statistics with QA, B9 and MLC

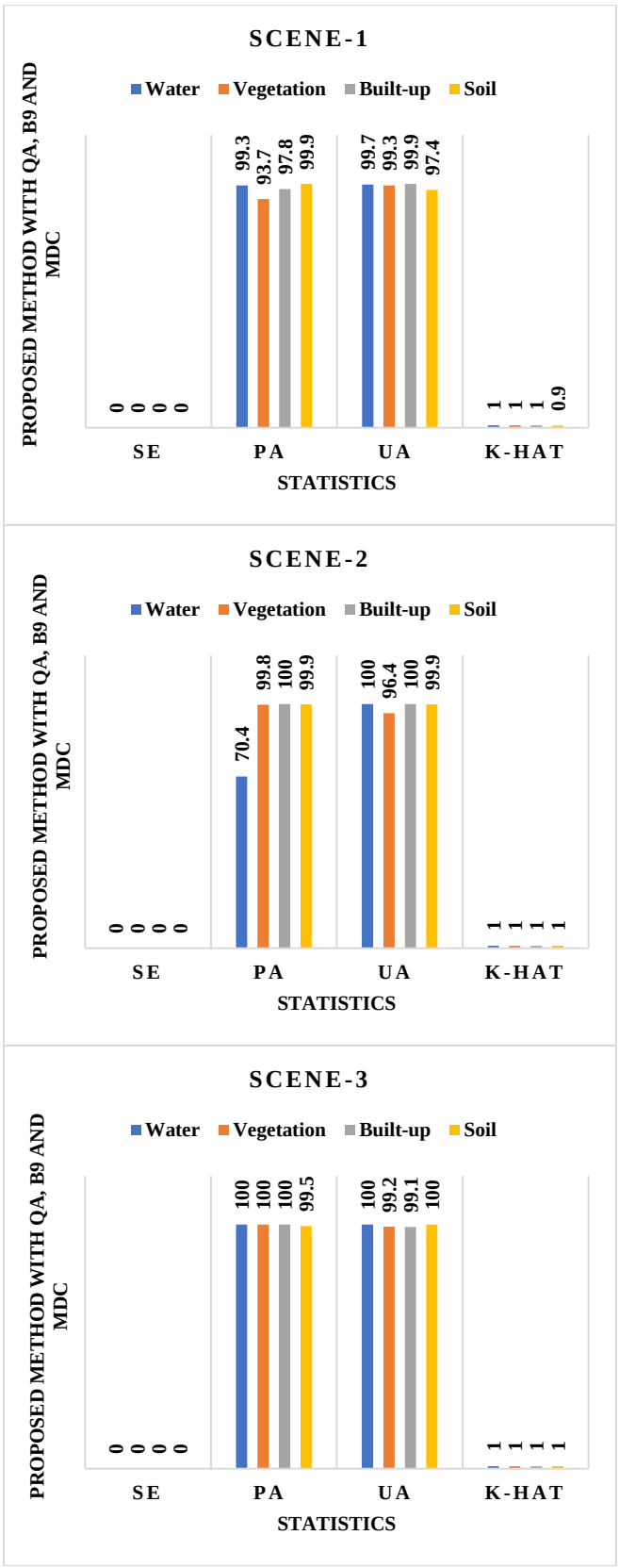

4 (b) Statistics with QA, B9 and MDC

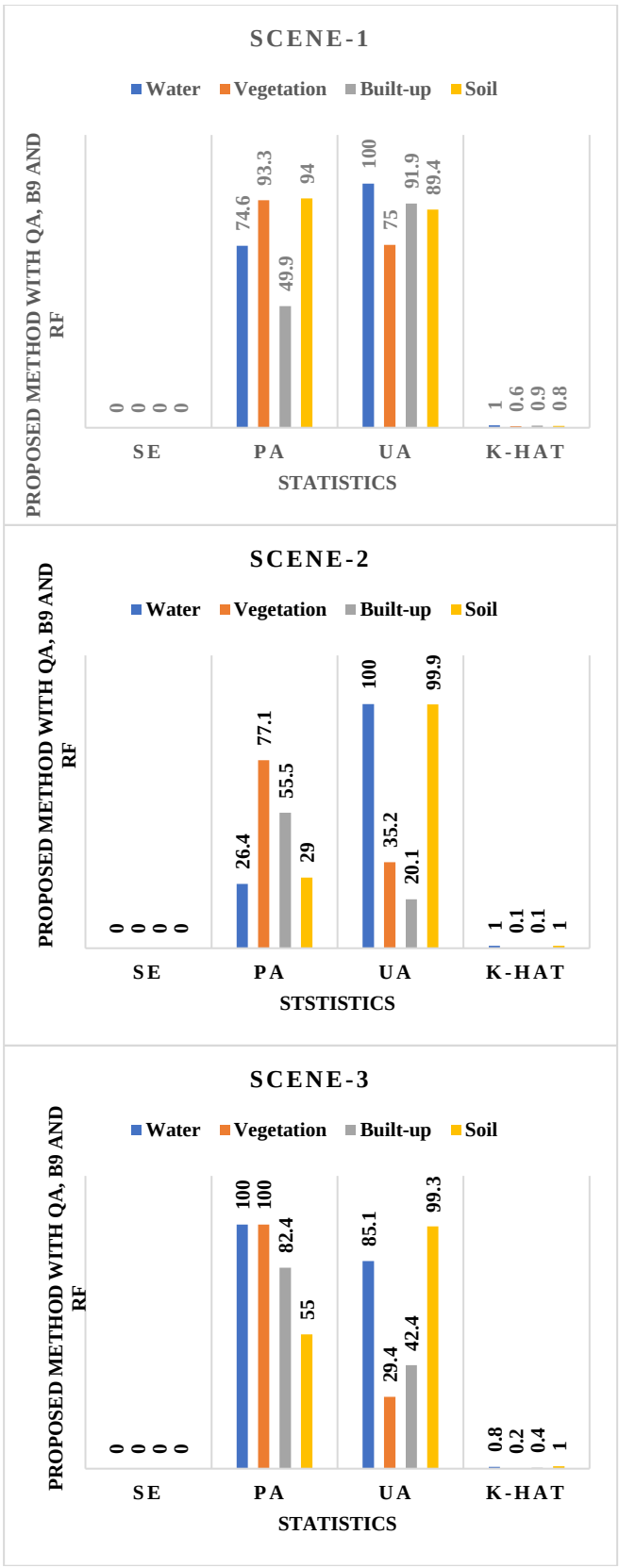

4 (c) Statistics with QA, B9 and RF

Fig. 4 Performance Metrics obtained for the proposed system with QA, B9 (MLC, MDC, RF)

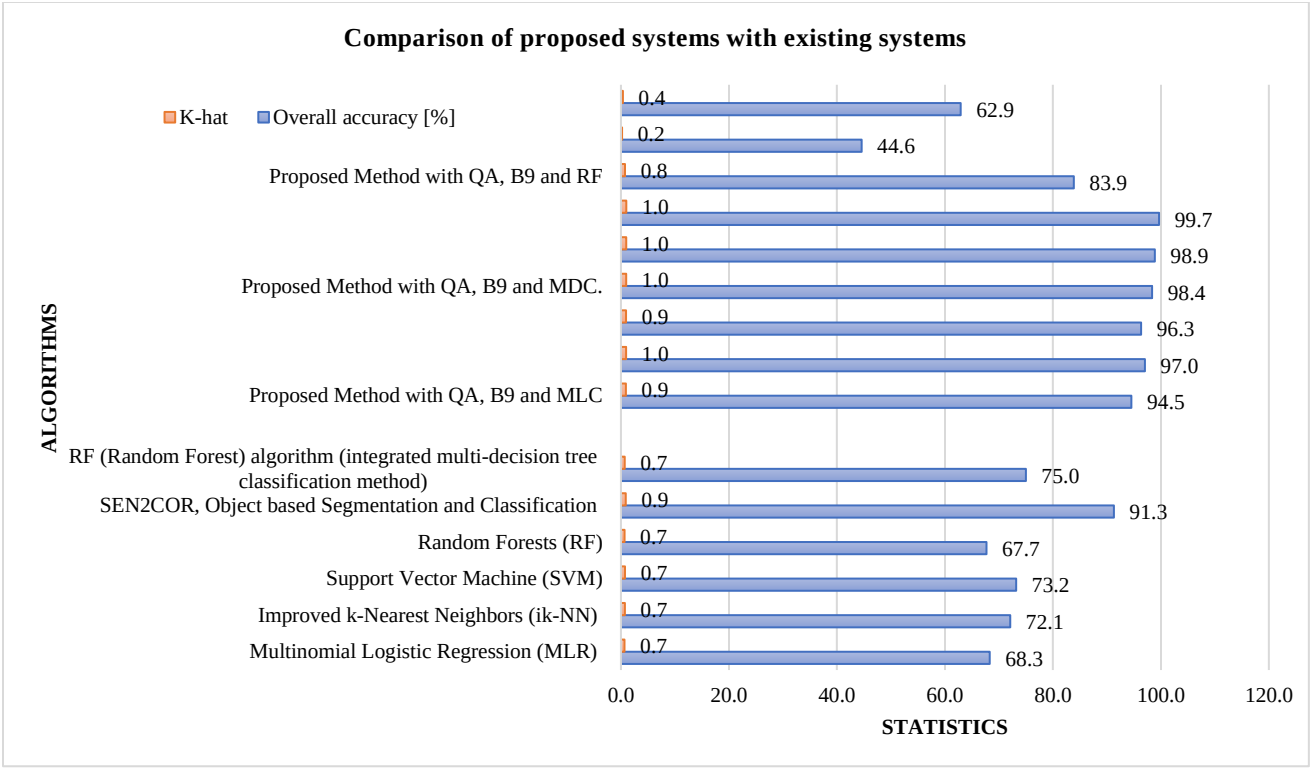

Fig. 5 Comparison of Performance Metrics obtained with the proposed system of cirrus, cloud and Shadow removal using QA, B9 (MLC, MDC, RF) and existing benchmark systems.

These are located in India and are referred to as Scene-1, Scene-2, and Scene-3, respectively. The proposed system of recognising and diminishing the cloud and shadow pixels produces the overall accuracies (%) for validation of ground truth with quality assessment band (QA), and B9 for Scene1, Scene 2, and Scene 3 using MLC are 94.5364, 97.0421, 96.3385; using MDC are 98.373, 98.8813, 99.6629 and using RF are 83.8781, 44.5804, and 62.9228. The k-hat achieved with the proposed system quality assessment band (QA) and B9 for Scene1, Scene 2, and Scene 3 using MLC are 0.9178, 0.9552, 0.9437, quality assessment band (QA) and B9 for Scene1, Scene 2, Scene 3 using MDC 0.973,0.9806, 0.9937, and quality assessment band (QA) and B9 for Scene1, Scene 2, Scene 3 using RF are 0.7509, 0.2083, 0.3631. The better result obtained with the proposed system when blended with MDC can be viewed in the comparison graph shown in fig. 5.

The varide statistics SE, PA, UA, and K-hat obtained with the proposed system of QA, B-9, with MLC, MDC and RF can be visualised through the graphical presentation displayed in fig.4. It can be observed from the graphs that the pixels collected with QA, B9 and MDC give the more accurate classification result. The outperformance of the proposed system with QA, B-9, MLC and MDC can be seen from the graph shown in Fig.4 and Fig. 5.

4. Conclusion

The proposed system identifies the climatic noise by using the combination of empirical pixel values of the Quality Assessment Band and Band-9 of LANSAT8/OLI/TIRS. Land cover is classified using Maximum Likelihood Classifier (MLC), Minimum Distance Classification (MDC), and Random Forest Classifier (RF) by using the threshold calculated with NDVI and NDWI.

The Land Cover is reconstructed after collecting and replacing the pixel values; comparing performance measurements with existing systems depicts the desired results achieved to validate ground truth.

The resultant OA percentage and reliability operator obtained with the proposed system when blended with MDC and MLC is better than the existing methods. The results obtained with QA, B-9 and RF are good for scene-1, but for scene-2 and scene-3, OA is not more than 80%, and k-hat is also not much closer to 1. So, it needs to add more samples and trees for accurate classification. This research can be carried forward for improving the classification obtained with QA, B-9 and RF algorithm, as the results achieved with this method may not be utilized for its applicability in the field of remote sensing.

References

[1] Daniel Schläpfer, Rudolf Richter, and Peter Reinartz, "Elevation-Dependent Removal of Cirrus Clouds in Satellite Imagery," *Remote Sensing*, vol. 12, no. 3, p. 494, 2020. *Crossref*, https://doi.org/10.3390/rs12030494

[2] Bo-Cai Gao, and Rong-Rong Li, "Removal of Thin Cirrus Scattering Effects in Landsat 8 OLI Images Using the Cirrus Detecting Channel," *Remote Sensing*, vol. 9, no. 8, p. 834, 2017. *Crossref*, https://doi.org/10.3390/rs9080834

[3] Binxing Zhou, and Yong Wang, "A Thin-Cloud Removal Approach Combining the Cirrus Band and RTM-Based Algorithm for Landsat-8 OLI Data," *IGARSS 2019 - 2019 IEEE International Geoscience and Remote Sensing Symposium*, pp. 1434-1437, 2019. *Crossref*, https://doi.org/10.1109/igarss.2019.8898644

[4] Yang Shen et al., "Removal of Thin Clouds in Landsat-8 OLI Data with Independent Component Analysis," *Remote Sensing*, vol. 7, pp. 11481-11500, 2015. *Crossref*, https://doi.org/10.3390/rs70911481

[5] Ratna Prastyani, and Abdul Basith, "Cirrus Cloud Correction in Landsat 8 Image Using the Image-Based Approach: A Case Study in Sumba Island, Indonesia," *2018 4th International Conference on Science and Technology (ICST)*, Yogyakarta, pp. 1-5, 2018. *Crossref*, https://doi.org/10.1109/ICSTC.2018.8528629

[6] Jing Wei et al., "Cloud Detection for Landsat Imagery by Combining the Random Forest and Superpixels Extracted via Energy-Driven Sampling Segmentation Approaches," *Remote Sensing of Environment*, vol. 248, p. 112005, 2020. *Crossref*, https://doi.org/10.1016/j.rse.2020.112005

[7] Nan Ma et al., "Cloud Detection Algorithm for Multi-Satellite Remote Sensing Imagery Based on a Spectral Library and 1D Convolutional Neural Network," *Remote Sensing*, vol. 13, no. 16, p. 3319, 2021. *Crossref*, https://doi.org/10.3390/rs13163319

[8] Lam Pham et al., "Remote Sensing Image Classification using Transfer Learning and Attention Based Deep Neural Network," *arXiv*, 2022. *Crossref*, https://doi.org/10.48550/arXiv.2206.13392

[9] Cengis Hasan et al., "Cloud Removal from Satellite Imagery Using Multispectral Edge-Filtered Conditional Generative Adversarial Networks," *International Journal of Remote Sensing*, vol. 43, no. 5, pp. 1881-1893, 2022. *Crossref*, https://doi.org/10.1080/01431161.2022.2048915

[10] Sergii Skakun et al., "Cloud Mask Intercomparison eXercise (CMIX): An Evaluation of Cloud Masking Algorithms for Landsat 8 and Sentinel-2," *Remote Sensing of Environment*, vol. 274, p. 112990, 2022. *Crossref*, https://doi.org/10.1016/j.rse.2022.112990

[11] Zhiwei Li et al., "Cloud and Cloud Shadow Detection for Optical Satellite Imagery: Features, Algorithms, Validation, and Prospects," *ISPRS Journal of Photogrammetry and Remote Sensing*, vol. 188, pp. 89-108, 2022. *Crossref*, https://doi.org/10.1016/j.isprsjprs.2022.03.020

[12] Hélène Chepfer et al., "Cirrus Cloud Properties Derived from POLDER-1/ADEOS Polarized Radiances: First Validation Using a Ground-Based Lidar Network," *Journal of Applied Meteorology*, vol. 39, pp. 154-168, 2000. *Crossref*, https://doi.org/10.1175/1520-0450(2000)039<0154:CCPDFP>2.0.CO;2

[13] Amy Tal Rose, Lance Sherry, and Donglian Sun, "Methodology and Case Study for Validation of Aircraft-Induced Clouds from Hyperspectral Imagery," *Atmosphere*, vol. 13, no. 8, p. 1257, 2022. *Crossref*, https://doi.org/10.3390/atmos13081257

[14] Tran Thi Ngoc Trieu et al., "Influences of Aerosols and Thin Cirrus Clouds on GOSAT XCO2 and XCH4 Using Total Carbon Column Observing Network, Sky Radiometer, and Lidar Data," *International Journal of Remote Sensing*, vol. 43, no. 5, pp. 1770-1799, 2022. *Crossref*, https://doi.org/10.1080/01431161.2022.2038395

[15] Qiang Li, and Silke Groß, "Satellite Observations of Seasonality and Long-Term Trend in Cirrus Cloud Properties over Europe: Investigation of Possible Aviation Impacts," *EGUsphere*, 2022. *Crossref*, https://doi.org/10.5194/egusphere-2022-628, 2022

[16] Saleem Ali et al., "Temporal and Vertical Distributions of the Occurrence of Cirrus Clouds over a Coastal Station in the Indian Monsoon Region," *Atmospheric Chemistry and Physics*, vol. 22, pp. 8321–8342, 2022. *Crossref*, https://doi.org/10.5194/acp-22-8321-2022.

[17] Shuang Liang et al., "Accurate Monitoring of Submerged Aquatic Vegetation in a Macrophytic Lake Using Time-Series Sentinel-2 Images," *Remote Sensing*, vol. 14, no. 3, p. 640, 2022. *Crossref*, https://doi.org/10.3390/rs14030640

[18] Junmei Kang et al., "Collaborative Extraction of Paddy Planting Areas with Multi-Source Information Based on Google Earth Engine: A Case Study of Cambodia," *Remote Sensing*, vol. 14, no. 8, p. 1823, 2022. *Crossref*, https://doi.org/ 10.3390/rs14081823

[19] Renuka S. Gound, and Dr. Sudeep D. Thepade, "Removal of Cloud and Shadow Influence from Remotely Sensed Images Through LANDSAT8/OLI/TIRS Using Minimum Distance Supervised Classification," *Indian Journal of Computer Science and Engineering*, vol. 12, pp. 1734-1748, 2021. *Crossref*, https://doi.org/10.21817/indjcse/2021/v12i6/211206118

[20] Y.Vishnu Tej et al., "A Novel Methodology for Denoising Impulse Noise in Satellite Images through Isolated Vector Median Filter with k-means Clustering," *International Journal of Engineering Trends and Technology*, vol. 70, no. 8, pp. 272-283, 2022. *Crossref*, https://doi.org/10.14445/22315381/IJETT-V70I8P229

[21] Huong Thi Thanh Nguyen et al., “Land Use/Land Cover Mapping Using Multitemporal Sentinel-2 Imagery and Four Classification Methods—A Case Study from Dak Nong, Vietnam,” *Remote Sensing*, vol. 12, no. 9, p. 1367, 2020. *Crossref*, https://doi.org/10.3390/rs12091367

[22] Yuhendra, and Eva Yulianti, “Multi-Temporal Sentinel-2 Images for Classification Accuracy,” *Journal of Computer Science*, vol. 15, no. 2, pp. 258-268, 2019. *Crossref*, https://doi.org/10.3844/jcssp.2019.258.268

[23] Ju Zeng et al., “Comparison of Landsat 8, Sentinel-2 and spectral indices combinations for Google Earth Engine-based land use mapping in the Johor River Basin, Malaysia,” *Malaysian Journal of Society and Space*, vol. 17, no. 3, 2021. *Crossref*, https://doi.org/10.17576/geo-2021-1703-03

[24] LANDSAT8. [Online]. Available: https://earthexplorer.usgs.gov/scene/metadata/full/5e81f14f59432a27/LC81440462018037LGN00/

[25] Aniekan Eyoh, and Francis Okeke, "Evaluation of the Relationship between Land Use/Land Cover Dynamics and Land Surface Temperature across the Niger Delta Region of Nigeria," *SSRG International Journal of Geoinformatics and Geological Science*, vol. 4, no. 3, pp. 1-12, 2017. *Crossref*, https://doi.org/10.14445/23939206/IJGGS-V4I5P101

[26] LANDSAT8. [Online]. Available: https://earthexplorer.usgs.gov/scene/metadata/full/5e81f14f59432a27/LC81440462018101LGN00

[27] Anish Anurag et al., "Local Attention-Based Descriptor Definition using Vision Transformer for Breast Cancer Identification," *International Journal of Engineering Trends and Technology*, vol. 70, no. 12, pp. 317-327, 2022. *Crossref*, https://doi.org/10.14445/22315381/IJETT-V70I12P230

[28] HB Kekre, Sudeep D Thepade, and Tejas Chopra, "Face and Gender Recognition Using Principal Component Analysis", *International Journal on Computer Science and Engineering*, vol. 2, no. 4, pp. 959-964, 2010.

[29] HB Kekre, Sudeep D Thepede, and Akshay Maloo, "Eigenvectors of Covariance Matrix using Row Mean and Column Mean Sequences for Face Recognition,” *International Journal of Biometrics and Bioinformatics*, vol. 4, no. 2, pp. 42-50, 2010.

[30] HB Kekre, Sudeep D Thepade, and Akshay Maloo, "Comprehensive Performance Comparison of Cosine, Walsh, Haar, Kekre, Sine, Slant and Hartley Transforms for CBIR with Fractional Coefficients of Transformed Image," *International Journal of Image Processing*, vol. 5, no. 3, pp. 336-351, 2011.

[31] HB Kekre, Sudeep D Thepade, and Parkar Adib, "An Extended Performance Comparison of Colour to Grey and Back using the Haar, Walsh, and Kekre Wavelet Transforms," *International Journal of Advanced Computer Science and Applications*, vol. 3, pp. 92-99, 2011. *Crossref*, https://doi.org/10.14569/SpecialIssue.2011.010315

[32] LANDSAT8. [Online]. Available: https://earthexplorer.usgs.gov/scene/metadata/full/5e81f14f59432a27/LC81440462018053LGN00/

[33] Renuka S. Gound, and Dr. Sudeep D. Thepade, “Validation of Ground Truth of Remotely Sensed Data from SENTINEL-2 (MSI) Using Supervised Classification, After Combined Cloud and Shadow Effect Removal,” *Indian Journal of Computer Science and Engineering*, vol. 13, pp. 860-868, 2022. *Crossref*, https://doi.org/10.21817/indjcse/2022/v13i3/221303164